ACS OMEGA

Open Access

http://pubs.acs.org/journal/acsodf

Article

Synthesis of pH-Sensitive Nitrogen-Doped Carbon Dots with Biological Imaging Function and Their Application in Cu^{2+} and Fe^{2+} Determination by Ratiometric Fluorescent Probes

Liucheng Guo, Luyao Li, Xingxian Wang, Yan Zhang,* and Fengling Cui*

Cite This: *ACS Omega* 2023, 8, 37098−37107

Read Online

ACCESS | Metrics & More | Article Recommendations | Supporting Information

ABSTRACT: pH-sensitive nitrogen-doped carbon dots (N-CDs) were synthesized using immature seeds of elm trees as a carbon source and ethylenediamine as a coreactant through a facile one-step hydrothermal method. The N-CDs were characterized using fluorescence spectroscopy, fluorescence lifetime, ultraviolet−visible absorption, X-ray photoelectron spectroscopy, X-ray diffraction, and Fourier transform infrared spectroscopy, as well as transmission electron microscopy. The N-CDs displayed excellent fluorescence properties and responded to pH changes. The N-CDs exhibited low toxicity and good biocompatibility and had the potential to be used for the biological imaging of HeLa cells and mung bean sprouts. Utilizing the mechanism of fluorescence resonance energy transfer, ratiometric fluorescent probes were prepared by simple mixing of N-CDs and fluorexon in a Britton−Robinson buffer solution. The ratiometric fluorescent probe was used to detect Cu^{2+} and Fe^{2+}. The linear equations were $R_{Cu} = -0.0591[Q] + 3.505$ ($R^2 = 0.992$) and $R_{Fe} = -0.0874[Q] + 3.61$ ($R^2 = 0.999$). The corresponding limits of detection were 0.5 and 0.31 μM, respectively. The good results had been obtained in the actual samples detection.

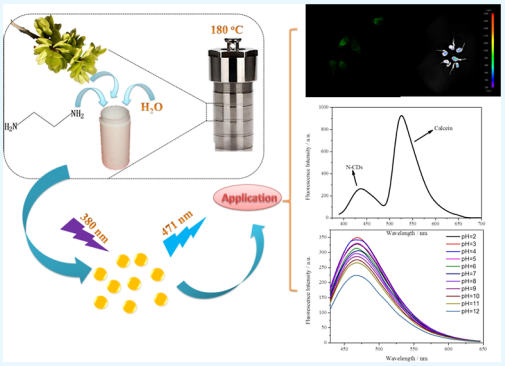

1. INTRODUCTION

Carbon dots (CDs) are carbon-based nanomaterials that have excellent optical properties, high chemical stability, good biocompatibility, and low toxicity; hence, they have broad application prospects in biological imaging,[1,2] sensing,[3−5] drug delivery,[6,7] and photocatalysis.[7,8] In this way, CDs have attracted increasing attention of researchers worldwide.[1,9] The methods for the preparation of CDs include arc discharge,[10,11] laser ablation,[12] electrochemical oxidation,[13] chemical oxidation,[14] microwave-assisted,[15−17] and hydrothermal[5,18,19] methods. Among them, the hydrothermal method is simple and eco-friendly and does not require a complicated technology or special equipment.[1,11] Eco-friendly carbon sources (eggs,[17] banana peel,[20] papaya seeds,[21] milk,[22,23] and leaves[24]) are widely used for the preparation of CDs.[19] Thus far, the application of CDs mainly in ion sensing and the use of pH-sensitive CDs have been reported rarely.[25]

However, nonproportional CDs probes are easily influenced by external factors, which hinders their practical applicability.[26] Ratiometric fluorescent probes can effectively avoid the influence of external factors and improve the determination accuracy.[27] Ratiometric fluorescent probes based on CDs have been prepared,[27,28] but no studies have assessed the utility of the ratiometric fluorescent probe to determine Cu^{2+} and Fe^{2+}. Many kinds of sensors based on heavy metal ions have gained popularity because of their low cost and avoidance of interference factors.[29−31]

In this paper, we prepared the distribution of pH-sensitive nitrogen-doped carbon dots (N-CDs) using immature seeds of elm trees (ISET) and ethylenediamine (EDA) through a one-step hydrothermal method. The N-CDs were applied for pH monitoring, bioimaging of cells and mung bean sprouts, and the fabrication of the ratiometric fluorescent probe with fluorexon because of the high fluorescence intensity, pH-sensitive behavior, low cytotoxicity, good biocompatibility, and high photo stability (Figure 1).

2. MATERIALS AND METHODS

2.1. Materials, Apparatus, and Characterization. N-CDs were characterized by transmission electron microscopy (TEM), X-ray photoelectron spectroscopy (XPS), UV−vis absorption, and fluorescence spectroscopy. The laser confocal microscope and small animal living imager were used for fluorescence imaging. For more information about materials,

Received: June 27, 2023
Accepted: September 13, 2023
Published: September 25, 2023

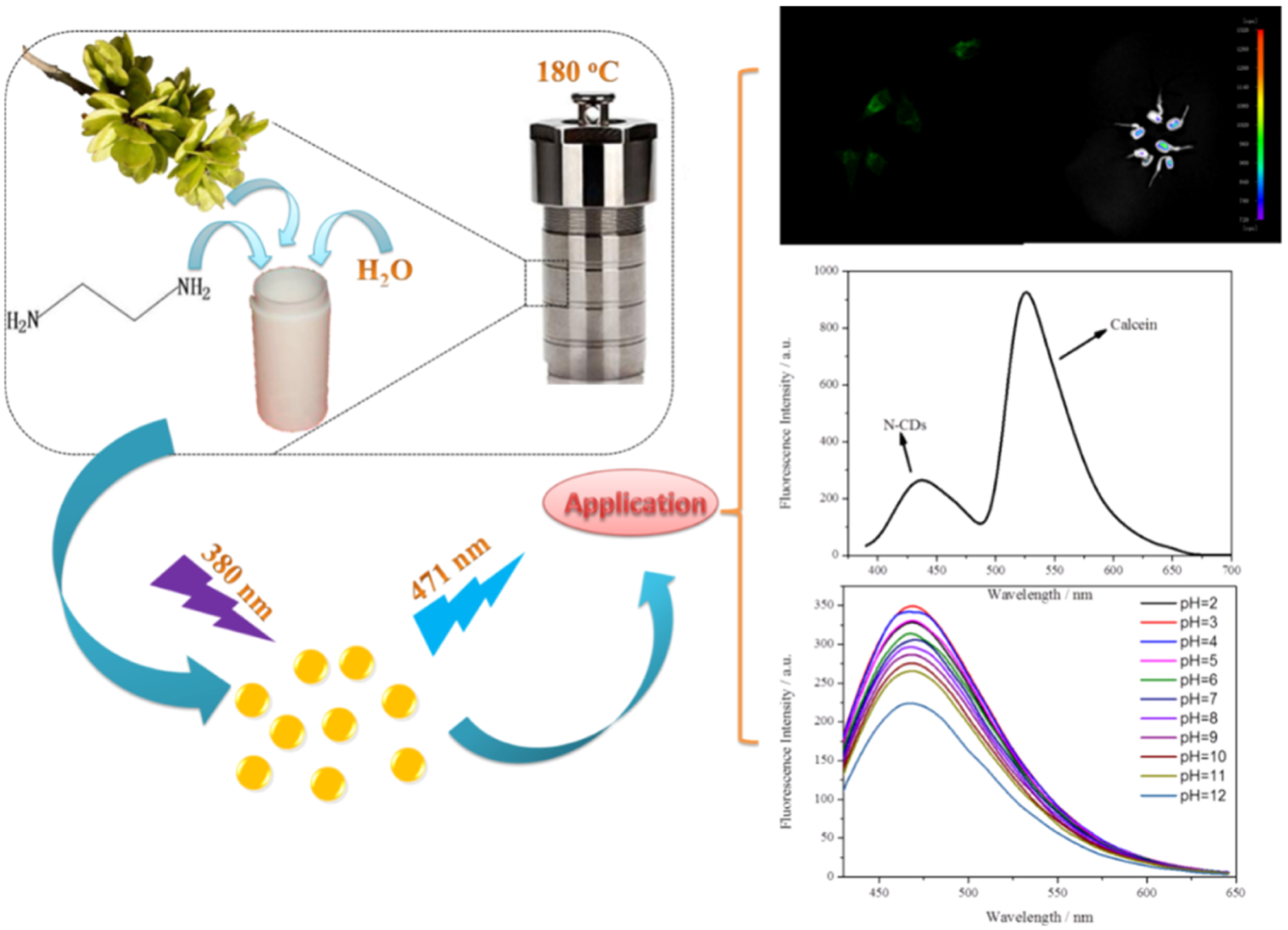

Figure 1. Schematic diagram of the synthesis of N-CDs and their application for pH monitoring, bioimaging, and fabrication of the ratiometric fluorescent probe.

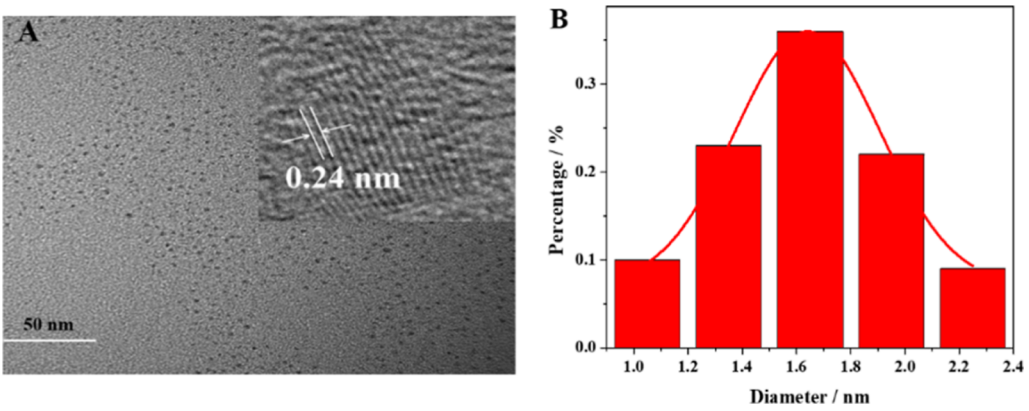

Figure 2. (A) TEM image of N-CDs. Inset: the high-resolution TEM image of N-CDs. (B) Size distribution of N-CDs.

apparatus, and characterization, please refer to the Supporting Information.

2.2. Synthesis of N-CDs. Briefly, 0.5 g of ISET powder, 25 μL of EDA, and 30 mL of double-distilled water were mixed and transferred to a Teflon-lined autoclave. The mixture was then heated to 180 °C for 15 h. A dark brown solution was obtained after being naturally cooled to room temperature. The solution was then centrifuged (12,000 rpm) for 20 min, and the filtrate was filtered through a 0.22 μm filter membrane to discard large-sized particles. The supernatant was dried and prepared into a 7 mg/mL N-CDs aqueous solution.

2.3. Fabrication of the Ratiometric Fluorescent Probe. The ratiometric fluorescent probe was prepared using synthesized N-CDs as the reference fluorophore and fluorexon as the test probe. Briefly, 100 μL of the prepared N-CDs solution was mixed with 48 μL of fluorexon (1 mM, dissolved in water) in 652 μL of Britton−Robinson (BR) buffer solution (pH = 6).

https://doi.org/10.1021/acsomega.3c04596
ACS Omega 2023, 8, 37098−37107

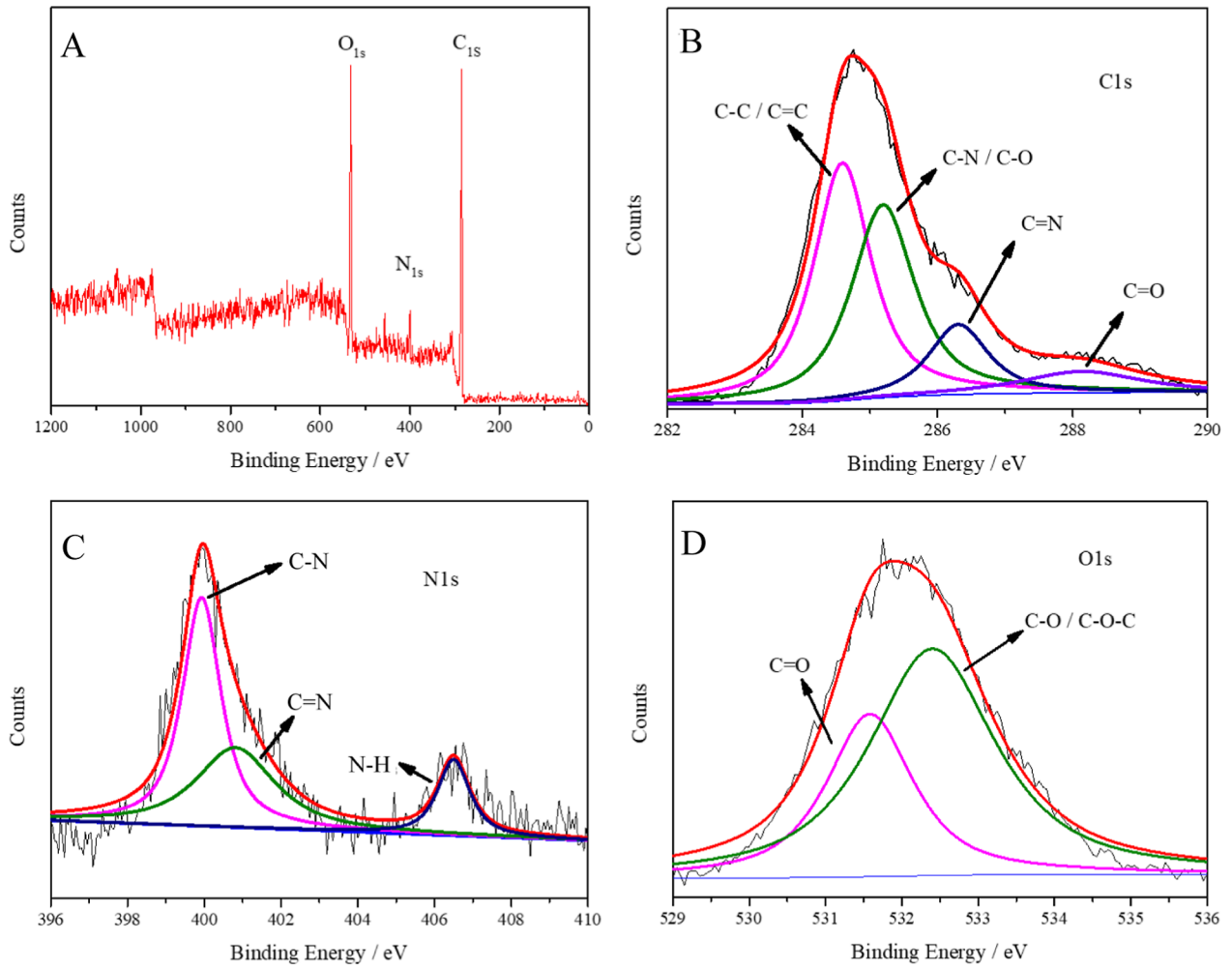

Figure 3. (A) XPS spectrum, (B) C 1s spectrum, (C) N 1s spectrum, and (D) O 1s spectrum of the N-CDs.

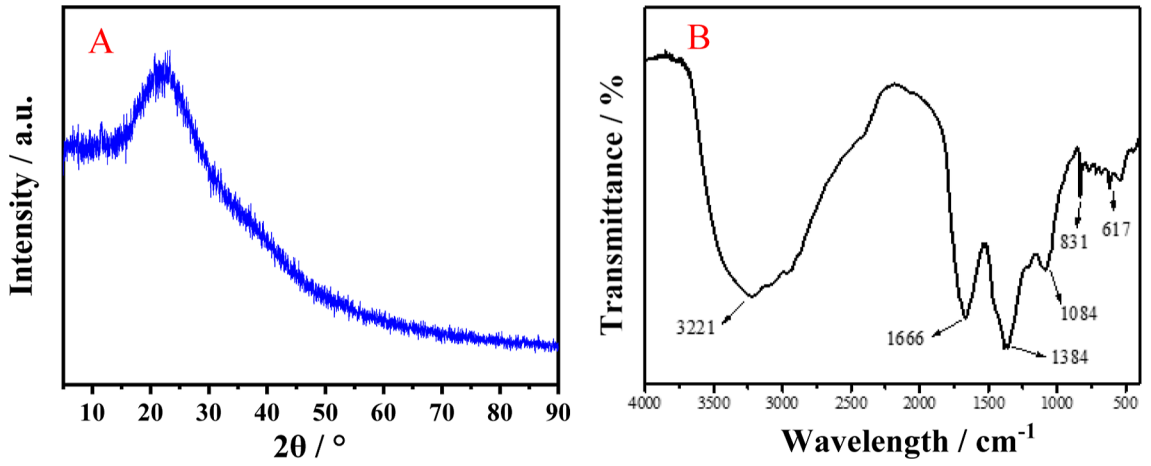

Figure 4. (A) X-ray diffraction pattern of N-CDs and (B) FTIR spectrum of N-CDs.

2.4. Analysis of Real-World Samples. $CuSO_4$ and $FeSO_4$ could be used as raw materials to prepare medical drugs and as feed additives to supplement iron and copper. The raw materials ($CuSO_4$ and $FeSO_4$), feed additives, and drugs were analyzed individually. After dilution, the amounts of Cu^{2+} and Fe^{2+} in the samples were determined using the probe and compared with the theoretical values. The determination accuracy of the results was evaluated by the relative error.

3. RESULTS AND DISCUSSION

3.1. Characterization. The results shown in Figure 2 confirmed that the prepared N-CDs were nearly spherical with a good size distribution of approximately 1−2.5 nm, and the average diameter was 1.64 nm. The TEM image (insert of Figure 2A) demonstrates that the lattice spacing of N-CDs was 0.24 nm, which corresponded with the spacing of the (100) planes of the graphite carbons.[24] As shown in Figure 4A, the X-

https://doi.org/10.1021/acsomega.3c04596
ACS Omega 2023, 8, 37098−37107

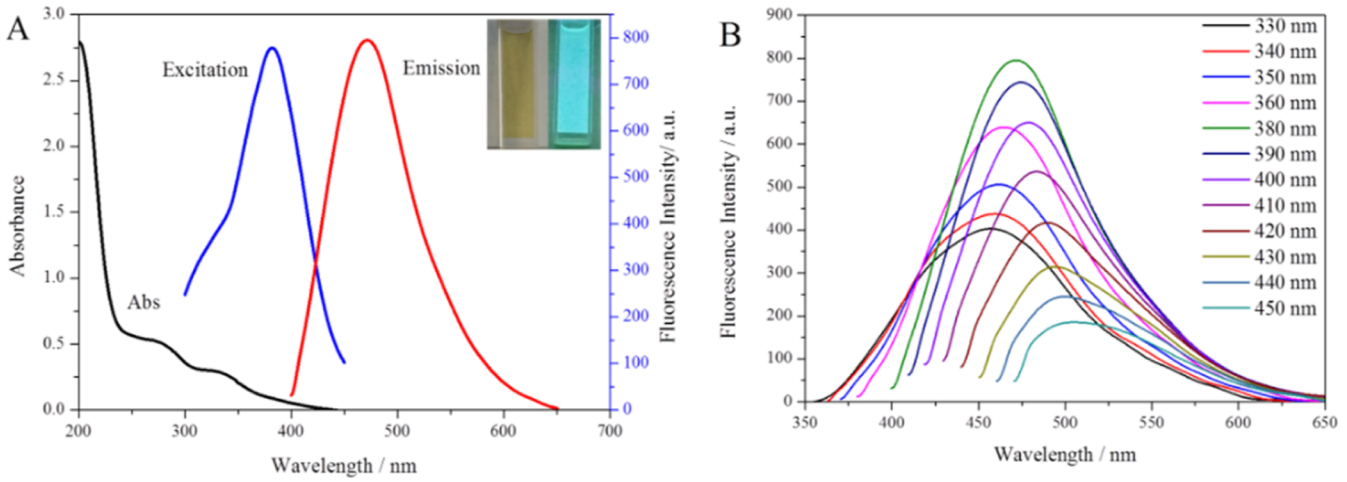

Figure 5. (A) UV−visible, excitation, and emission spectra of N-CDs. Inset: N-CDs under sunlight (left) and 365 nm UV light (right). (B) Fluorescence spectra of the N-CDs at different excitation wavelengths.

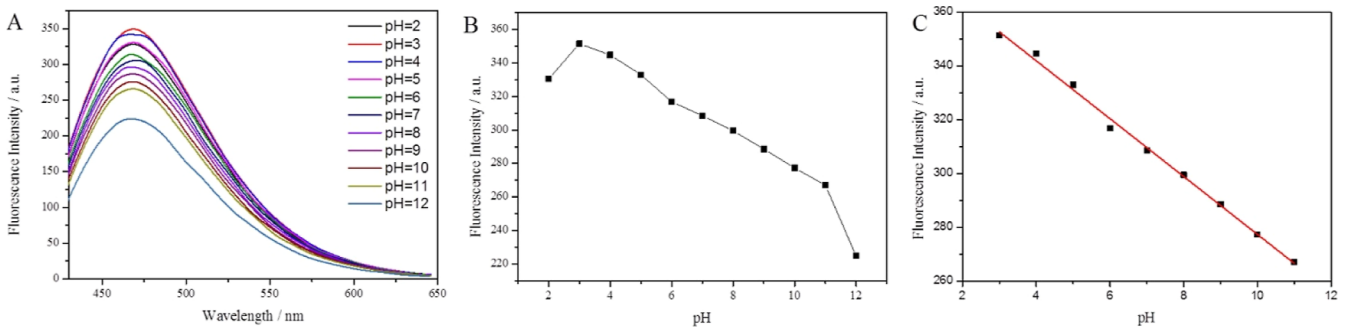

Figure 6. (A) Fluorescence spectra of the N-CDs at different pH values. (B) Fluorescence intensity of N-CDs at different pH values. (C) Linear relationship between the fluorescence intensity and pH.

ray diffraction patterns of N-CDs had a broad peak centered at ≈23°, which corresponded to the (100) interplanar spacing of the graphite and was consistent with the TEM results.[32]

The surface groups on N-CDs were studied from XPS and Fourier transform infrared (FTIR) spectra. The XPS results showed that the N-CDs comprised C (68.02%), N (9.83%), and O (22.15%), indicating the successful synthesis of N-CDs. The XPS spectra had three peaks of C 1s, N 1s, and O 1s at 306.0, 400.0, and 611.0 eV, respectively (Figure 3A). In the C 1s spectrum, four peaks were observed at 284.6, 285.15, 286.3, and 288.1 eV, corresponding to C−C/C═C, C−N/C−O, C═N, and C═O, respectively.[17,33] According to the N 1s spectrum, the three peaks at 399.93, 400.81, and 406.5 eV belonged to C−N, C═N, and N−H, respectively.[34] In the O 1s spectrum, two peaks were observed at 531.58 and 532.40 eV, corresponding to C═O and C−O/C−O−C, respectively.[17,35] XPS results showed that the surface of the N-CDs had an abundance of the −COOH, $-NH_2$, and −OH groups.

As shown in Figure 4B, the broad absorption peak at 3221 cm^{-1} was attributed to the stretching vibrations of O−H and N−H.[35,36] The peaks at 1666 and 1384 cm^{-1} were assigned to the C═O[17] and C═N stretching vibrations, respectively.[24] Moreover, characteristic C−H bending vibrations at 1084 cm^{-1} were observed in the spectrum.[17] The FTIR spectrum suggested the existence of −COOH, $-NH_2$, and −OH groups on the surface of N-CDs, consistent with the results of XPS.

3.2. Optical Properties of N-CDs. As shown in Figure 5A (black line), the N-CDs had two absorption peaks around 270 and 330 nm, attributed to $\pi-\pi^*$ and $n-\pi^*$ transitions, respectively.[7,37] N-CDs with cyan emission under 365 nm ultraviolet (UV) light had an excitation wavelength of 380 nm and an emission wavelength of 471 nm (Figure 5A). N-CDs exerted an excitation-dependent fluorescence behavior and had the maximum emission when the excitation wavelength was 380 nm (Figure 5B).[38] The excitation-dependent behavior was caused by the energy trap on the surface of the N-CDs.[37] In addition, the quantum yield of N-CDs was 5.16% when quinine sulfate was used as the reference, and the lifetime was 5.44 ns (Figure S1).

The influence of the concentration, ionic strength, metal ions, and negative ions on the fluorescence intensity of N-CDs was further studied to gain a better understanding of N-CDs' fluorescence properties. As shown in Figure S2A, the fluorescence intensity of N-CDs was the highest at a dose of 0.7 mg/mL, and this concentration was chosen in the experiment. Ions (50 μM) had a minimal effect on N-CDs (Figures S3C,D). The results showed that the synthesized N-CDs had good stability. N-CDs had the potential to be used in biological imaging and ratiometric fluorescent probes.

3.3. Sensitivity of N-CDs for pH Detection. Figure 6A,B shows the fluorescence spectrum and intensity of N-CDs in BR buffer over a wide pH range (pH 2−12). When the pH range is 3−12, the fluorescence intensity decreased, and the prepared N-CDs were pH-sensitive. As shown in Figure 6C, the fluorescence intensity showed a strong linear relationship with pH in the pH range of 3−11. The equation was $F = -10.92$ pH

https://doi.org/10.1021/acsomega.3c04596
ACS Omega 2023, 8, 37098−37107

+ 388.02, wherein F values represent the N-CDs' fluorescence intensity and the R^2 value is 0.996. Therefore, the N-CDs obtained could be used for pH detection. The pH-sensitivity property of N-CDs was attributed to the protonation and deprotonation of $-NH_2$ and $-COOH$ on the surface of N-CDs.[39] When the pH value increased from 3 to 11, the degree of deprotonation of the N-CDs increased, consequently reducing the fluorescence intensity. The pH-sensitive property of N-CDs could be exploited for pH monitoring in biological and biomedical applications.

3.4. Cell Cytotoxicity of N-CDs and Their Bioimaging Application. Cell cytotoxicity was evaluated by using the MTT method before the bioimaging experiment. As shown in Figure S3, cell viability was greater than 84% even when the concentration of N-CDs reached 2 mg/mL, suggesting that the N-CDs were weakly toxic and had the potential to be used as a fluorescent probe for biological imaging applications. Therefore, N-CDs were exposed to HeLa cells and mung bean sprouts to assess their biological imaging ability. HeLa cells and mung bean sprouts were treated with 1 and 2 mg/mL N-CDs for 12 h and 3 weeks, respectively. As shown in Figure 7B, HeLa cells emitted bright green fluorescence, which indicated that N-CDs entered into HeLa cells. As shown in Figure 7C–F, compared with mung bean sprouts cultured in double-distilled water, those cultured in N-CDs emitted bright fluorescence. The results showed that N-CDs with low biological toxicity and good biocompatibility could be used for biological imaging of HeLa cells and mung bean sprouts.

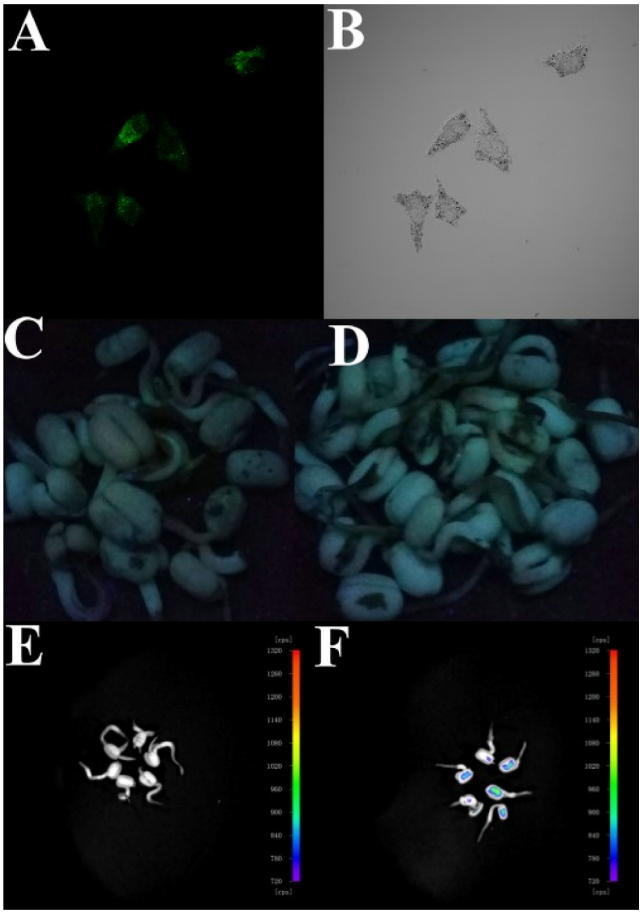

Figure 7. Images of HeLa cells at λ_{ex} = 405 nm (A) and bright-field images (B) with N-CDs. The photographs of mung bean sprouts cultured with double-distilled water (C) and after treatment with 2 mg/mL N-CDs (D) under a UV lamp (λ_{ex} = 365 nm). The images of mung bean sprouts cultured with double-distilled water (E) and treated with 2 mg/mL N-CDs (F) under a live animal imager (λ_{ex} = 405 nm).

3.5. Fabrication of the Ratiometric Fluorescent Probe. Using photostable N-CDs and fluorexon as the reference fluorophore, a ratiometric fluorescent probe was prepared. To study the interaction between N-CDs and fluorexon, different amounts of fluorexon were added into the N-CD solution of a certain concentration, and the fluorescence intensities of N-CDs and fluorexon were measured. As shown in Figure 8, the fluorescence intensity of the N-CDs at around 470 nm decreased gradually with the increasing fluorexon concentration. When the fluorexon concentration reached 10 μM, two obvious emission peaks were observed in the fluorescence spectra. As shown in Figure 8B, when the concentration exceeded 60 μM, the change in the fluorescence intensity of fluorexon became slow. Therefore, a 60 μM concentration was selected. As shown in Figure 8C, a good linear relationship was observed between the fluorescence intensity of N-CDs, and the fluorexon concentration range was 10–40 μM.

The effect of the pH on the system was also investigated (Figure S4). The ratiometric fluorescence of fluorexon to N-CDs was the highest at pH 5. However, the fluorescence spectrum of the system at pH 6 was better than that at pH 5. Therefore, the pH of solution was set at 6.

3.6. Mechanism of the Ratiometric Fluorescent Probe. To study the mechanism of the ratiometric fluorescent probe composed of N-CDs and fluorexon, the fluorescence spectra of N-CDs, fluorescein, and the system of N-CDs and fluorescein were measured. As shown in Figure 9A, the fluorescence intensity of fluorexon in the system was higher than that of fluorexon alone, which indicated the fluorescence resonance energy transfer between N-CDs and fluorexon. As shown in Figure 9B, a great overlap existed between the emission spectrum of N-CDs and the absorption spectrum of fluorexon, suggesting a fluorescence resonance energy transfer between N-CDs and fluorexon.

3.7. Ratiometric Fluorescence Assay of $Cu^{2+}$and Fe^{2+}. Different metal ions (50 μM) were added to study the sensing ability. The results showed that only Cu^{2+} and Fe^{2+} could change the ratio of the probe (R), which indicated that N-CDs could be used as a ratiometric fluorescent probe (Figure S5).

As shown in Figure 10A, R decreased with the increase in the Cu^{2+} concentration. In the range of 0.6–40 μM, a good linear relationship was observed between R and Cu^{2+} concentration (Q) (Figure 10B). The linear relationship was $R = -0.0591[Q] + 3.505$ (R^2 = 0.992), and the limit of detection (LOD) was 0.50 μM. Similarly, as shown in Figure 11, a good linear curve could be obtained between R and Fe^{2+} concentration (Q) in the concentration range of 0.4–8 μM. The linear relationship and LOD were $R = -0.0874[Q] + 3.61$ (R^2 = 0.999) and 0.31 μM, respectively. Compared with the reported probes, the probe had better linearity and a wider linear range (Table S1).

3.8. Quenching Mechanism of the Ratiometric Fluorescence Probe. The UV–vis spectrum and fluorescence lifetime were measured to study the quenching mechanism of ratiometric probes by Cu^{2+} and Fe^{2+}. As shown in Figure 12A,B, after addition of quenchers (Cu^{2+} or Fe^{2+}), the UV–vis spectrum of the probe + Cu^{2+} (or Fe^{2+})

https://doi.org/10.1021/acsomega.3c04596
ACS Omega 2023, 8, 37098–37107

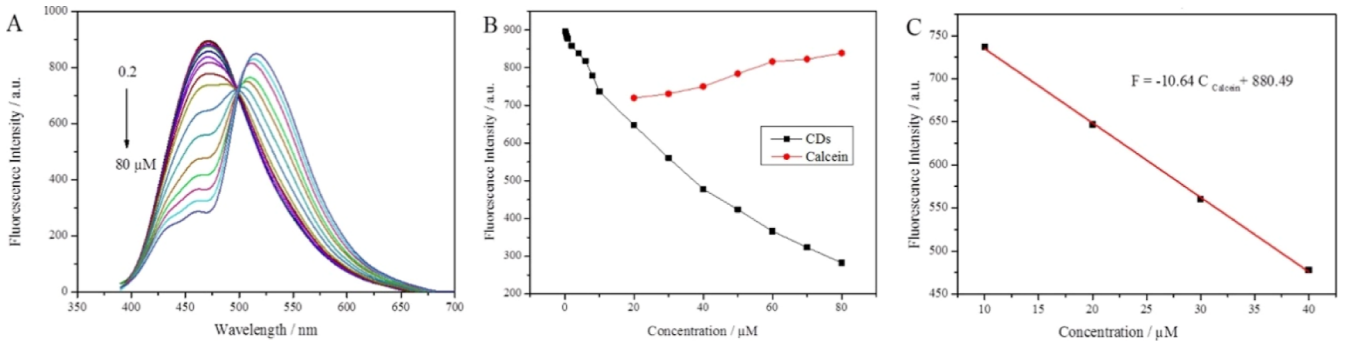

Figure 8. (A) Fluorescence spectra of the N-CDs in different concentrations of fluorexon: 0.2, 0.4, 0.6, 0.8, 1.0, 2.0, 4.0, 6.0, 8.0, 10, 20, 30, 40, 50, 60, 70, and 80 μM. (B) Changes in fluorescence intensity of N-CDs and fluorexon. (C) Linear relationship of the ratiometric fluorescent probe (10−40 μM).

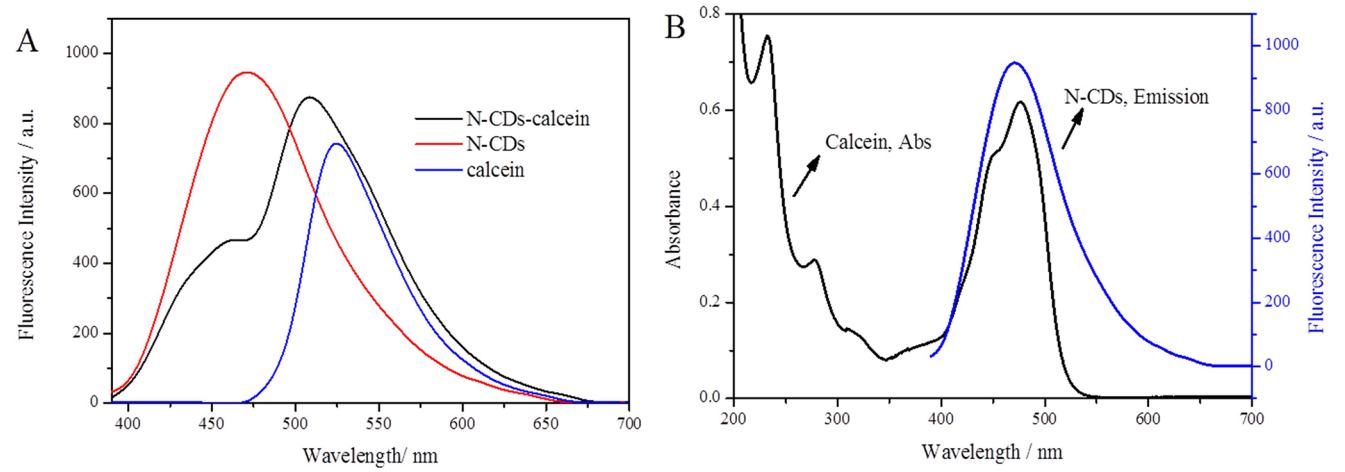

Figure 9. (A) Fluorescence spectra of N-CDs, fluorexon, and the N-CDs−fluorexon probe. (B) Absorbance spectrum of fluorexon and emission spectrum of N-CDs.

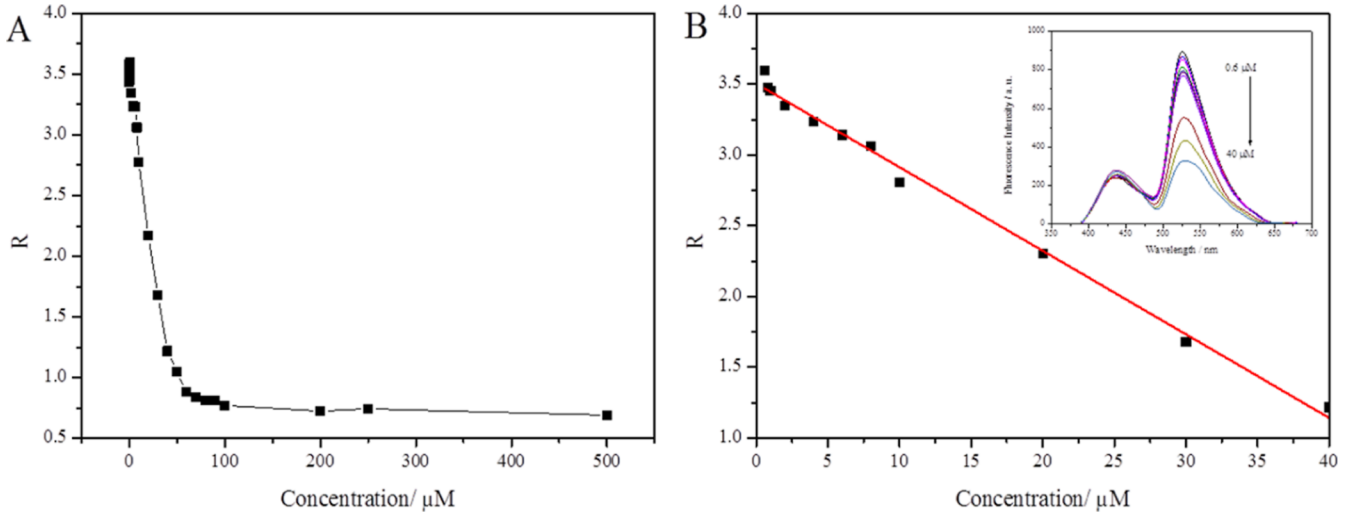

Figure 10. (A) Fluorescence response of the ratiometric probe at different Cu^{2+} concentrations (0, 0.004, 0.008, 0.02, 0.04, 0.06, 0.08, 0.10, 0.20, 0.40, 0.60, 0.80, 1.0, 2.0, 4.0, 6.0, 8.0, 10, 20, and 40 μM). (B) Linear relationship between R and Cu^{2+}. Inset: emission spectrum of the ratiometric probe in different Cu^{2+} concentrations.

system was the sum of the spectra of the probe and the quencher, and no new absorption peak appeared. As shown in Figure 12C,D, the fluorescence lifetime of the probe system did not change significantly after the quenchers were added, indicating dynamic quenching.

3.9. Determination of $Cu^{2+}$and Fe^{2+}in Real-World Samples. To explore the applicability, we used the ratiometric probe to determine Cu^{2+} and Fe^{2+} in real-world samples. The concentrations of Cu^{2+} and Fe^{2+} in actual samples were calculated by using the linear equation. As shown in Table 1,

https://doi.org/10.1021/acsomega.3c04596
ACS Omega 2023, 8, 37098−37107

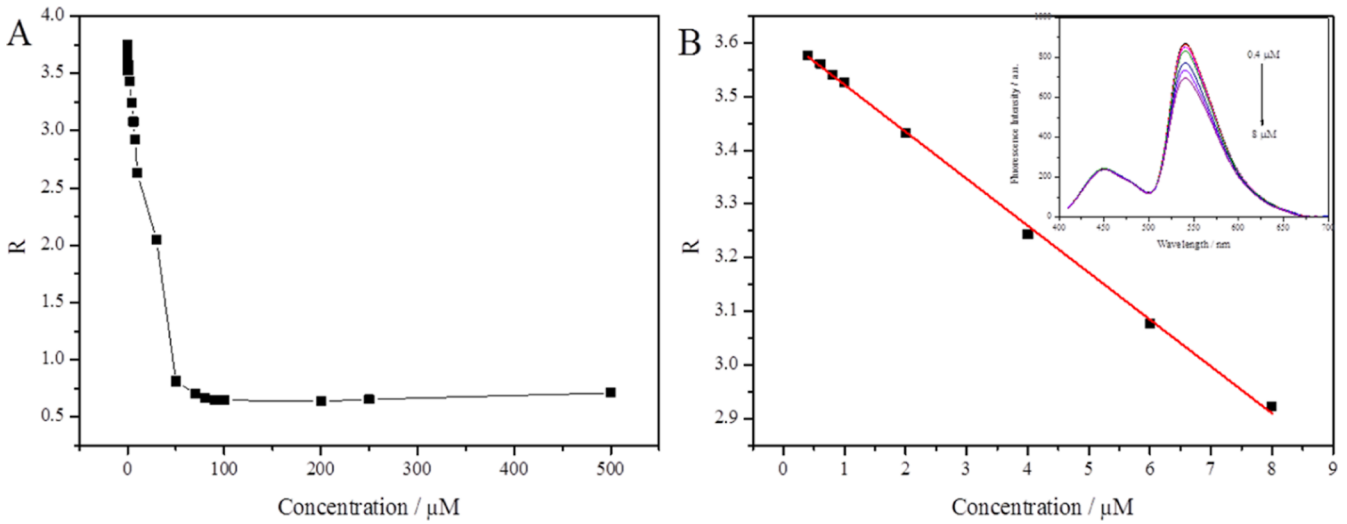

Figure 11. (A) Fluorescence response of the ratiometric probe at different Fe^{2+} concentrations (0, 0.004, 0.008, 0.02, 0.04, 0.06, 0.08, 0.10, 0.20, 0.40, 0.60, 0.80, 1.0, 2.0, 4.0, 6.0, 8.0, 10, 20, and 40 μM). (B) Liner relationship of R and Fe^{2+} concentration in the concentration range of 0.4−8.0 μM. Inset: emission spectrum of the ratiometric probe at different Fe^{2+} concentrations.

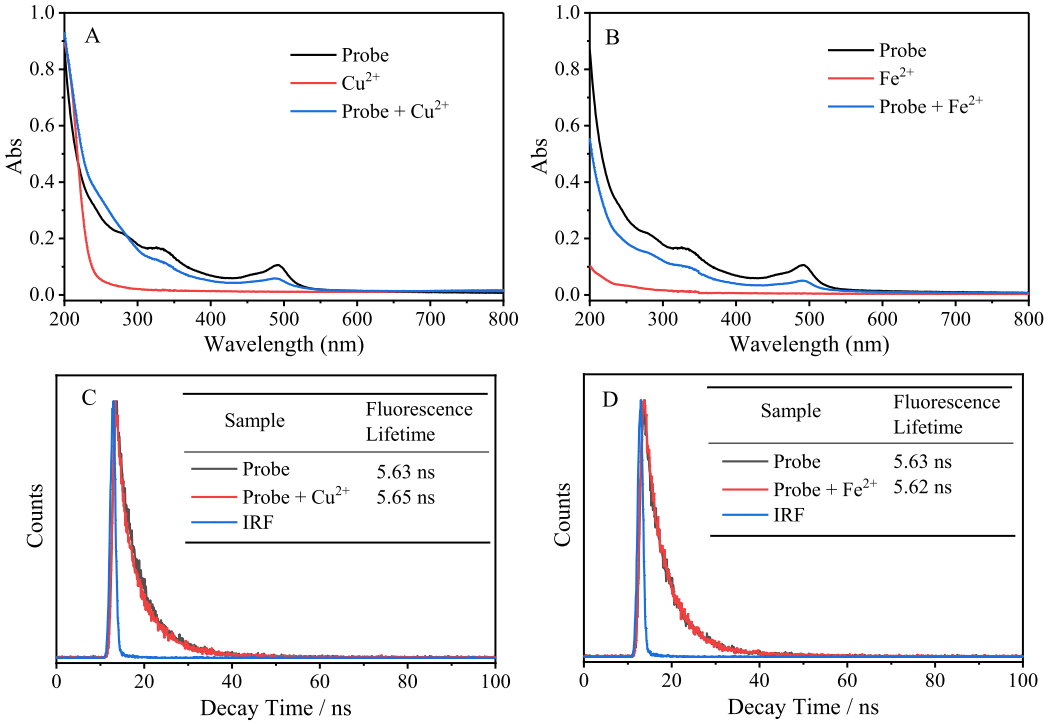

Figure 12. (A) UV−vis absorption of the probe, Cu^{2+}, and probe + Cu^{2+}, (B) UV−vis absorption of the probe, Fe^{2+}, and probe + Fe^{2+}, (C) fluorescence decay traces of the probe and probe + Cu^{2+}, and (D) fluorescence decay traces of the probe and probe + Fe^{2+}.

the probe could be used to detect Cu^{2+} and Fe^{2+} in actual samples. The measured values were approximate to the theoretical values, and the relative errors were less than 1%, which indicated that the established method was reliable for determination in practical samples.

4. CONCLUSIONS

The hydrothermal method is simple and suitable for the large-scale synthesis of N-CDs. The pH-sensitive N-CDs with a size of 1.64 nm, a quantum yield of 5.1%, and a lifetime of 5.44 ns were obtained by using the simple hydrothermal carbonization method. Carbon sources of N-CDs (ISET and EDA) were eco-friendly. Fortunately, N-CDs have excellent properties such as high fluorescence intensity, pH sensitivity, low cytotoxicity, good biocompatibility, and high light stability. Therefore, the N-CDs can be used for pH monitoring, biological imaging of cells and mung bean sprouts, and the preparation of fluorescent probes with the ratiometric fluorescence of Fe^{2+} and Cu^{2+}. Specifically, the N-CDs had a good fluorescence response to pH at a pH range of 2−11 and were used as a fluorescent sensor for pH monitoring. The N-CDs exhibited weak toxicity to both plants and cells and have the potential to be used in the biomedical field. In addition, the ratiometric fluorescence probe had a simple design, did not need special

https://doi.org/10.1021/acsomega.3c04596
ACS Omega 2023, 8, 37098−37107

Table 1. Application of Probes in Real-World Samples (n = 3)

actual sample	probe	theoretical content (mg)	measured content (mg)	RSD (%)	relative error (%)[b]
$CuSO_4$ raw material drugs	Cu^{2+}	5.0	5.02	1.00	0.4
$CuSO_4$ solution[a]	Cu^{2+}	5.0	5.00	0.30	0.0
$CuSO_4$ feed additive	Cu^{2+}	5.0	5.01	0.16	0.2
$FeSO_4$ raw material drugs	Fe^{2+}	5.0	4.99	1.50	0.2
$FeSO_4$ tablets	Fe^{2+}	5.0	5.03	0.34	0.6
ferrous lactate tablets	Fe^{2+}	5.0	4.97	0.88	0.6

[a]$CuSO_4$ solution is a raw material produced by Zhonglian Chemical Reagent Co., Ltd. in Tianjin, China, for scientific experiments and the production of Bordeaux mixtures. [b]Relative error = |measured content − theoretical content| ÷ theoretical content × 100%.

instruments and harsh conditions, and could avoid more interference; thus, the ratiometric fluorescent probe was used to simultaneously detect Cu^{2+} and Fe^{2+} with LODs of 0.50 and 0.31 μM, respectively, as it had more advantages than other sensing methods.

■ ASSOCIATED CONTENT

Supporting Information

The Supporting Information is available free of charge at https://pubs.acs.org/doi/10.1021/acsomega.3c04596.

Fluorescence decays of the N-CDs (Ex: 405 nm and Em: 471 nm); influence of the concentration of N-CDs on fluorescence intensity; effect of ionic strength, metal ions, and negative ions on the fluorescence intensity of N-CDs; cell viability of Hela cells after incubation with various concentrations of N-CDs; R of the ratiometric fluorescent probe at different pH values; fluorescence spectra of system (N-CDs-Fluorexon) at pH values of 5 and 6; effect of ionic strength on the R of the ratiometric fluorescent probe; and the determination operation methods including the measurement of the fluorescence quantum yield, cytotoxicity assays, sensitivity of the N-CDs for pH detection, bioimaging, and metal ions sensing test of the ratiometric fluorescent probe (PDF)

■ AUTHOR INFORMATION

Corresponding Authors

Yan Zhang − *College of Food and Biological Engineering, Henan University of Animal Husbandry and Economy, Zhengzhou, Henan 450000, P. R. China;* orcid.org/0000-0002-6234-4365; Email: zhybio@outlook.com

Fengling Cui − *Collaborative Innovation Center of Henan Province for Green Manufacturing of Fine Chemicals, Key Laboratory of Green Chemical Media and Reactions, Ministry of Education, National Demonstration Center for Experimental Chemistry Education, Henan Engineering Laboratory for Bioconversion Technology of Functional Microbes, School of Chemistry and Chemical Engineering, Henan Normal University, Xinxiang 453007, P. R. China;* orcid.org/0000-0002-0413-3084; Email: fenglingcui@hotmail.com

Authors

Liucheng Guo − *Collaborative Innovation Center of Henan Province for Green Manufacturing of Fine Chemicals, Key Laboratory of Green Chemical Media and Reactions, Ministry of Education, National Demonstration Center for Experimental Chemistry Education, Henan Engineering Laboratory for Bioconversion Technology of Functional Microbes, School of Chemistry and Chemical Engineering, Henan Normal University, Xinxiang 453007, P. R. China; Luohe Medical College, Luohe 462000, P. R. China*

Luyao Li − *Collaborative Innovation Center of Henan Province for Green Manufacturing of Fine Chemicals, Key Laboratory of Green Chemical Media and Reactions, Ministry of Education, National Demonstration Center for Experimental Chemistry Education, Henan Engineering Laboratory for Bioconversion Technology of Functional Microbes, School of Chemistry and Chemical Engineering, Henan Normal University, Xinxiang 453007, P. R. China; College of Advanced Interdisciplinary Science and Technology, Henan University of Technology, Zhengzhou 450001, P. R. China*

Xingxian Wang − *Collaborative Innovation Center of Henan Province for Green Manufacturing of Fine Chemicals, Key Laboratory of Green Chemical Media and Reactions, Ministry of Education, National Demonstration Center for Experimental Chemistry Education, Henan Engineering Laboratory for Bioconversion Technology of Functional Microbes, School of Chemistry and Chemical Engineering, Henan Normal University, Xinxiang 453007, P. R. China*

Complete contact information is available at: https://pubs.acs.org/10.1021/acsomega.3c04596

Author Contributions

Conceptualization, L.G. and L.L.; writing—original draft preparation, L.G. and L.L.; writing—review and editing, L.G., L.L., X.W., Y.Z. and F.C.; investigation, L.G., L.L., and F.C.; and supervision, Y.Z. and F.C. All authors have read and agreed to the published version of the manuscript.

Notes

The authors declare no competing financial interest.

■ ACKNOWLEDGMENTS

This research was funded by National Natural Science Foundation of China (U1704170) and the Key Programs for Science and Technology Development in Henan Province (212102110164 and 222102110130).

■ REFERENCES

(1) Yu, Y.; Zeng, Q.; Tao, S.; Xia, C.; Liu, C.; Liu, P.; Yang, B. Carbon Dots Based Photoinduced Reactions: Advances and Perspective. *Adv. Sci.* **2023**, *10* (12), 2207621.

(2) Shen, C.; Liu, H.; Lou, Q.; Wang, F.; Liu, K.; Dong, L.; Shan, C. Recent Progress of Carbon Dots in Targeted Bioimaging and Cancer Therapy. *Theranostics* **2022**, *12* (6), 2860−2893.

(3) Hou, J.; Dong, J.; Zhu, H.; Teng, X.; Ai, S.; Mang, M. A Simple and Sensitive Fluorescent Sensor for Methyl Parathion Based on L-Tyrosine Methyl Ester Functionalized Carbon Dots. *Biosens. Bioelectron.* **2015**, *68*, 20−26.

(4) Ajith, M. P.; Pardhiya, S.; Rajamani, P. Carbon Dots: An Excellent Fluorescent Probe for Contaminant Sensing and Remediation. *Small* **2022**, *18* (15), 2105579.

(5) Lu, W.; Guo, Y.; Yue, Y.; Zhang, J.; Fan, L.; Li, F.; Zhao, Y.; Dong, C.; Shuang, S. Smartphone-Assisted Colorimetric Sensing

Platform Based on Molybdenum-Doped Carbon Dots Nanozyme for Visual Monitoring of Ampicillin. *Chem. Eng. J.* **2023**, *468*, 143615.
(6) Hou, L.; Chen, D.; Wang, R.; Wang, R.; Zhang, H.; Zhang, Z.; Nie, Z.; Lu, S. Transformable Honeycomb-like Nanoassemblies of Carbon Dots for Regulated Multisite Delivery and Enhanced Antitumor Chemoimmunotherapy. *Angew. Chem., Int. Ed.* **2021**, *60* (12), 6581−6592.
(7) Liang, Y.; Gou, S.; Liu, K.; Wu, W.; Guo, C. Z.; Lu, S. Y.; Zang, J.; Wu, X.; Lou, Q.; Dong, L.; Gao, Y.; Shan, C. Ultralong and Efficient Phosphorescence from Silica Confined Carbon Nanodots in Aqueous Solution. *Nano Today* **2020**, *34*, 100900.
(8) Rosso, C.; Filippini, G.; Prato, M. Carbon Dots as Nano-Organocatalysts for Synthetic Applications. *ACS Catal.* **2020**, *10* (15), 8090−8105.
(9) Wang, B.; Waterhouse, G. I. N.; Lu, S. Carbon Dots: Mysterious Past, Vibrant Present, and Expansive Future. *Trends in Chem.* **2023**, *5* (1), 76−87.
(10) Dey, S.; Govindaraj, A.; Biswas, K.; Rao, C. N. R. Luminescence Properties of Boron and Nitrogen Doped Graphene Quantum Dots Prepared from Arc-Discharge-Generated Doped Graphene Samples. *Chem. Phys. Lett.* **2014**, *595*−*596*, 203−208.
(11) Ge, G.; Li, L.; Wang, D.; Chen, M.; Zeng, Z.; Xiong, W.; Wu, X.; Guo, C. Carbon Dots: Synthesis, Properties and Biomedical Applications. *J. Mater. Chem. B* **2021**, *9* (33), 6553−6575.
(12) Hu, S.; Liu, J.; Yang, J.; Wang, Y.; Cao, S. Laser Synthesis and Size Tailor of Carbon Quantum Dots. *J. Nanopart. Res.* **2011**, *13* (12), 7247−7252.
(13) Du, X.; Zhang, M.; Ma, Y.; Wang, X.; Liu, Y.; Huang, H.; Kang, Z. Size-Dependent Antibacterial of Carbon Dots by Selective Absorption and Differential Oxidative Stress of Bacteria. *J. Colloid Interface Sci.* **2023**, *634*, 44−53.
(14) Qin, F.; Li, Q.; Tang, T.; Zhu, J.; Gan, X.; Chen, Y.; Li, Y.; Zhang, S.; Huang, X.; Jia, D. Functional Carbon Dots from a Mild Oxidation of Coal Liquefaction Residue. *Fuel* **2022**, *322*, 124216.
(15) Zhang, Y.; Wang, L.; Hu, Y.; Sui, L.; Cheng, L.; Lu, S. Centralized Excited States and Fast Radiation Transitions Reduce Laser Threshold in Carbon Dots. *Small* **2023**, *19*, 2207983.
(16) Yetiman, S.; Peçenek, H.; Dokan, F. K.; Onses, M. S.; Yılmaz, E.; Sahmetlioglu, E. Microwave-Assisted Fabrication of High-Performance Supercapacitors Based on Electrodes Composed of Cobalt Oxide Decorated with Reduced Graphene Oxide and Carbon Dots. *J. Energy Storage* **2022**, *49*, 104103.
(17) Yu, L.; He, M.; Liu, S.; Dou, X.; Li, L.; Gu, N.; Li, B.; Liu, Z.; Wang, G.; Fan, J. Fluorescent Egg White-Based Carbon Dots as a High-Sensitivity Iron Chelator for the Therapy of Nonalcoholic Fatty Liver Disease by Iron Overload in Zebrafish. *ACS Appl. Mater. Interfaces* **2021**, *13* (46), 54677−54689.
(18) Liu, K.; Guo, Y.; Yu, H.; Cheng, Y.; Xie, Y.; Yao, W. Sulfhydryl-Functionalized Carbon Dots as Effective Probes for Fluorescence Enhancement Detection of Patulin. *Food Chem.* **2023**, *420*, 136037.
(19) Fang, M.; Wang, B.; Qu, X.; Li, S.; Huang, J.; Li, J.; Lu, S.; Zhou, N. State-of-the-Art of Biomass-Derived Carbon Dots: Preparation, Properties, and Applications. *Chin. Chem. Lett.* **2023**, 108423.
(20) Das, M.; Thakkar, H.; Patel, D.; Thakore, S. Repurposing the Domestic Organic Waste into Green Emissive Carbon Dots and Carbonized Adsorbent: A Sustainable Zero Waste Process for Metal Sensing and Dye Sequestration. *J. Environ. Chem. Eng.* **2021**, *9* (5), 106312.
(21) Laddha, H.; Yadav, P.; Sharma, M.; Agarwal, M.; Gupta, R. Waste to Value Transformation: Converting Carica Papaya Seeds into Green Fluorescent Carbon Dots for Simultaneous Selective Detection and Degradation of Tetracycline Hydrochloride in Water. *Environ. Res.* **2023**, *227*, 115820.
(22) Wang, D.; Wang, X.; Guo, Y.; Liu, W.; Qin, W. Luminescent Properties of Milk Carbon Dots and Their Sulphur and Nitrogen Doped Analogues. *RSC Adv.* **2014**, *4* (93), 51658−51665.
(23) Mohamed, R. M. K.; Mohamed, S. H.; Asran, A. M.; Alsohaimi, I. H.; Hassan, H. M. A.; Ibrahim, H.; El-Wekil, M. M. Bifunctional Ratiometric Sensor Based on Highly Fluorescent Nitrogen and Sulfur Biomass-Derived Carbon Nanodots Fabricated from Manufactured Dairy Product as a Precursor. *Spectrochim. Acta, Part A* **2023**, *293*, 122444.
(24) Liu, Q.; Gao, X.; Liu, Z.; Gai, L.; Yue, Y.; Ma, H. Sensitive and Selective Electrochemical Detection of Lead(II) Based on Waste-Biomass-Derived Carbon Quantum Dots@zeolitic Imidazolate Framework-8. *Materials* **2023**, *16* (9), 3378.
(25) Gao, J.; Zhu, M.; Huang, H.; Liu, Y.; Kang, Z. Advances, Challenges and Promises of Carbon Dots. *Inorg. Chem. Front.* **2017**, *4* (12), 1963−1986.
(26) Huang, S.; Wang, L.; Zhu, F.; Su, W.; Sheng, J.; Huang, C.; Xiao, Q. A Ratiometric Nanosensor Based on Fluorescent Carbon Dots for Label-Free and Highly Selective Recognition of DNA. *RSC Adv.* **2015**, *5* (55), 44587−44597.
(27) Fan, Y.; Shen, L.; Liu, Y.; Hu, Y.; Long, W.; Fu, H.; She, Y. A Sensitized Ratiometric Fluorescence Probe Based on N/S Doped Carbon Dots and Mercaptoacetic Acid Capped CdTe Quantum Dots for the Highly Selective Detection of Multiple Tetracycline Antibiotics in Food. *Food Chem.* **2023**, *421*, 136105.
(28) Dai, R.; Chen, X.; Hu, Y. Ratiometric Fluorescence Determination of Carbon Disulfide in Water Using Surface Functionalized Carbon Dots. *Sens. Actuators, B* **2023**, *382*, 133499.
(29) Mohandoss, S.; Ahmad, N.; Khan, M. R.; Velu, K. S.; Palanisamy, S.; You, S.; Kumar, A. J.; Lee, Y. R. Nitrogen and Sulfur Co-Doped Photoluminescent Carbon Dots for Highly Selective and Sensitive Detection of Ag^{+} and Hg^{2+} Ions in Aqueous Media: Applications in Bioimaging and Real Sample Analysis. *Environ. Res.* **2023**, *228*, 115898.
(30) Liu, J.; Lv, G.; Gu, W.; Li, Z.; Tang, A.; Mei, L. A Novel Luminescence Probe Based on Layered Double Hydroxides Loaded with Quantum Dots for Simultaneous Detection of Heavy Metal Ions in Water. *J. Mater. Chem. C* **2017**, *5* (20), 5024−5030.
(31) Miao, P.; Tang, Y.; Wang, L. DNA Modified Fe_3O_4@Au Magnetic Nanoparticles as Selective Probes for Simultaneous Detection of Heavy Metal Ions. *ACS Appl. Mater. Interfaces* **2017**, *9* (4), 3940−3947.
(32) Zhang, Y.; Li, M.; Lu, S. Rational Design of Covalent Bond Engineered Encapsulation Structure toward Efficient, Long-lived Multicolored Phosphorescent Carbon Dots. *Small* **2023**, *19* (31), 2206080.
(33) Pang, C.; Cao, X.; Xiao, Y.; Luo, S.; Chen, Q.; Zhou, Y. J.; Wang, Z. N-Alkylation Briefly Constructs Tunable Multifunctional Sensor Materials: Multianalyte Detection and Reversible Adsorption. *iScience* **2021**, *24* (10), 103126.
(34) Fu, R.; Song, H.; Liu, X.; Zhang, Y.; Xiao, G.; Zou, B.; Waterhouse, G. I. N.; Lu, S. Disulfide Crosslinking-Induced Aggregation: Towards Solid-State Fluorescent Carbon Dots with Vastly Different Emission Colors. *Chin. J. Chem.* **2023**, *41* (9), 1007−1014.
(35) Wang, H.; Yang, Z.; Liu, Z.; Wan, J.; Xiao, J.; Zhang, H. Facile Preparation of Bright-Fluorescent Soft Materials from Small Organic Molecules. *Chem.—Eur. J.* **2016**, *22* (24), 8096−8104.
(36) Atchudan, R.; Edison, T. N. J. I.; Lee, Y. R. Nitrogen-Doped Carbon Dots Originating from Unripe Peach for Fluorescent Bioimaging and Electrocatalytic Oxygen Reduction Reaction. *J. Colloid Interface Sci.* **2016**, *482*, 8−18.
(37) Yun, S.; Kang, E. S.; Choi, J. Zn-Assisted Modification of the Chemical Structure of N-Doped Carbon Dots and Their Enhanced Quantum Yield and Photostability. *Nanoscale Adv.* **2022**, *4* (8), 2029−2035.
(38) Atchudan, R.; Edison, T. N. J. I.; Aseer, K. R.; Perumal, S.; Karthik, N.; Lee, Y. R. Highly Fluorescent Nitrogen-Doped Carbon Dots Derived from Phyllanthus Acidus Utilized as a Fluorescent Probe for Label-Free Selective Detection of Fe^{3+} Ions, Live Cell Imaging and Fluorescent Ink. *Biosens. Bioelectron.* **2018**, *99*, 303−311.
(39) Zhang, Q.; Wang, R.; Feng, B.; Zhong, X.; Ostrikov, K. Photoluminescence Mechanism of Carbon Dots: Triggering High-

https://doi.org/10.1021/acsomega.3c04596
ACS Omega 2023, 8, 37098−37107

Color-Purity Red Fluorescence Emission through Edge Amino Protonation. *Nat. Commun.* **2021**, *12* (1), 6856.

https://doi.org/10.1021/acsomega.3c04596
ACS Omega 2023, 8, 37098−37107